Aspects and consequences of a dressed-quark-gluon vertex

M. S. Bhagwat,[1] A. Höll,[2] A. Krassnigg,[2] C. D. Roberts,[2,3] and P. C. Tandy
[1]*Center for Nuclear Research, Department of Physics, Kent State University, Kent, Ohio 44242, USA*
[2]*Physics Division, Argonne National Laboratory, Argonne, Illinois 60439-4843, USA*
[3]*Fachbereich Physik, Universität Rostock, D-18051 Rostock, Germany*
(Received 2 March 2004; published 24 September 2004)

Features of the dressed-quark-gluon vertex and their role in the gap and Bethe-Salpeter equations are explored. It is argued that quenched lattice data indicate the existence of net attraction in the color-octet projection of the quark-antiquark scattering kernel. The study employs a vertex model whose diagrammatic content is explicitly enumerable. That enables the systematic construction of a vertex-consistent Bethe-Salpeter kernel and thereby an exploration of the consequences for the strong interaction spectrum of attraction in the color-octet channel. With rising current-quark mass the rainbow-ladder truncation is shown to provide an increasingly accurate estimate of a bound state's mass. Moreover, the calculated splitting between vector and pseudoscalar meson masses vanishes as the current-quark mass increases, which argues for the mass of the pseudoscalar partner of the $\Upsilon(1S)$ to be above 9.4 GeV. With the amount of attraction suggested by lattice data color-antitriplet diquarks are absent from the strong interaction spectrum.

DOI: 10.1103/PhysRevC.70.035205 PACS number(s): 12.38.Aw, 11.30.Rd, 12.38.Lg, 12.40.Yx

I. INTRODUCTION

Dynamical chiral symmetry breaking (DCSB) impacts materially on the strong interaction spectrum. For example, this phenomenon, which can even be expressed in models that omit confinement [1–3], is responsible for the remarkably small value of the ratio of π- and ρ-meson masses and, inseparable from this, the generation of large constituent-like masses for dressed-quarks. It follows both: That a sum of constituent-like dressed-quark masses sets a baseline for the masses of all light hadrons, except the pseudoscalar mesons; and that pseudoscalar "meson cloud" contributions are essential to an understanding of hadron observables, such as the masses [4,5] and form factors [6] of octet and decuplet baryons.

That stated, herein a primary concern is the dressed-quark-gluon vertex, $\Gamma^a_\nu(q;p)$. We are generally interested in its form, how that arises, and the ways it affects and is affected by strong interaction phenomena. The vertex is a key element in the gap equation[1]

$$S(p)^{-1} = Z_2(i\gamma\cdot p + m^{\rm bm}) + Z_1\int_q^\Lambda g^2 D_{\mu\nu}(p-q)\frac{\lambda^a}{2}\gamma_\mu S(q)\Gamma^a_\nu(q,p), \quad (1)$$

and this brings an immediate link with DCSB. The gap equation has long been used as a tool for developing insight into the origin of DCSB, and searching for a connection between DCSB and confinement [7]. Moreover, the vertex is essential to a valid description of bound states and therefore to realising and understanding Goldstone's theorem, and current conservation in general.

The gap equation also consists of: $D_{\mu\nu}(k)$, the renormalized dressed-gluon propagator; $m^{\rm bm}$, the Λ-dependent current-quark bare mass; and $\int_q^\Lambda := \int d^4q/(2\pi)^4$, which represents a translationally invariant regularization of the integral, with Λ the regularization mass-scale. The quark-gluon-vertex and quark wave function renormalization constants, $Z_{1,2}(\zeta^2,\Lambda^2)$, respectively, depend on Λ, the renormalization point, ζ, and the gauge parameter.

The gap equation's solution is the dressed-quark propagator, which takes the form

$$S(p)^{-1} = i\gamma\cdot pA(p^2,\zeta^2) + B(p^2,\zeta^2) = \frac{1}{Z(p^2,\zeta^2)}[i\gamma\cdot p + M(p^2,\zeta^2)]. \quad (2)$$

It provides direct access to the gauge invariant vacuum quark condensate [8–10]

$$-\langle\overline{q}q\rangle^0_\zeta = \lim_{\Lambda\to\infty} Z_4(\zeta^2,\Lambda^2)N_c{\rm tr}_{\rm D}\int_q^\Lambda S^0(q,\zeta). \quad (3)$$

In Eq. (3): Z_4 is the renormalization constant for the scalar part of the quark self-energy, through which the current-quark bare-mass is related to the running mass

$$Z_2(\zeta^2,\Lambda^2)m^{\rm bm}(\Lambda) = Z_4(\zeta^2,\Lambda^2)m(\zeta), \quad (4)$$

${\rm tr}_D$ identifies a trace over Dirac indices alone; and the superscript "0" indicates the quantity was calculated in the chiral limit, which is unambiguously defined in an asymptotically free theory [8–10].

It is a longstanding prediction of Dyson-Schwinger equation (DSE) studies [7,11,12] that the two-point Schwinger functions which characterize the propagation of QCD's elementary excitations are strongly dressed at infrared length-scales, namely, $k^2 \lesssim 2$ GeV^2; and it has become apparent that this feature is materially important in explaining a wide range of hadron properties [13].

[1](We employ a Euclidean metric, with: $\{\gamma_\mu,\gamma_\nu\}=2\delta_{\mu\nu}$; $\gamma_\mu^\dagger=\gamma_\mu$; and $a\cdot b=\sum_{i=1}^4 a_i b_i$.)

Such dressing is also a feature of the dressed-quark-gluon vertex, a three-point function, and it is certain that the infrared structure of this vertex has an impact on properties of the gap equation's solution, such as: Multiplicative renormalizability [14–16]; gauge covariance [15,17], and the existence and realization of confinement and DCSB [1–3,18–20]. For example, related vertex Ansätze, which agree in the ultraviolet, can yield solutions for the dressed-quark propagator via the gap equation with completely different analytic properties and incompatible conclusions on DCSB [21,22].

Dyson-Schwinger equation predictions for the behavior of dressed-gluon [23–25] and dressed-quark propagators; e.g., [9,19,20], have been confirmed in numerical simulations of lattice-regularized QCD [26,27]. Detailed study provides an understanding of the circumstances in which pointwise agreement is obtained [28]. This level of sophistication does not yet prevail with the quark-gluon vertex but is a realizable contemporary goal.

In Sec. II, we recapitulate on a nonperturbative DSE truncation scheme [29,30] that has already enabled some systematic study of the connection between the dressed-quark-gluon vertex and the expression of symmetries in strong interaction observables. In doing this we are led to propose an extension of earlier work, one which facilitates an exploration of the impact that aspects of the three-gluon vertex have on hadron phenomena. To amplify the illustrative efficacy of our analysis we introduce a simple model to describe the propagation of dressed-gluons [31] that reduces the relevant DSEs to a set of coupled algebraic equations which, notwithstanding their simplicity, exhibit characteristics essential to the strong interaction.

In Sec. III we chronicle features of the dressed-quark-gluon vertex and dressed-quark propagator that are common to our model and QCD. Of particular interest are the effects of net attraction in the color-octet quark-antiquark scattering kernel which we are able to identify. We follow that in Sec. IV with an analysis of the Bethe-Salpeter equations which can be constructed, consistent with the fully dressed-quark-gluon vertex, so that the Ward-Takahashi identities associated with strong interaction observables are automatically satisfied. This property is crucial to understanding hadron properties and interactions [8,32–35]. Section IV also contains an analysis of color-antitriplet diquark correlations.

We close our presentation with a summary in Sec. V.

II. DRESSED QUARK-GLUON VERTEX

A. General features

This Schwinger function can be calculated in perturbation theory but, since we are interested in the role it plays in connection with confinement, DCSB and bound state properties, that is inadequate for our purposes: These phenomena are essentially nonperturbative. Instead we begin by observing that the dressed vertex can be written

$$i\Gamma^a_\mu(p,q) = \frac{i}{2}\lambda^a\Gamma_\mu(p,q) =: l^a\Gamma_\mu(p,q), \tag{5}$$

viz., the color structure factorizes, and that twelve Lorentz invariant functions are required to completely specify the remaining Dirac-matrix-valued function; i.e.,

$$\Gamma_\mu(p,q) = \gamma_\mu\hat{\Gamma}_1(p,q) + \gamma\cdot(p+q)(p+q)_\mu\hat{\Gamma}_2(p,q) - i(p+q)_\mu\hat{\Gamma}_3(p,q) + [\ldots], \tag{6}$$

where the ellipsis denotes contributions from additional Dirac matrix structures that play no part herein. Since QCD is renormalizable, the bare amplitude associated with γ_μ is the only function in Eq. (6) that exhibits an ultraviolet divergence at one-loop in perturbation theory.

The requirement that QCD's action be invariant under local color gauge transformations entails [36]

$$k_\mu i\Gamma_\mu(p,q) = \mathcal{F}^g(k^2)\{[1-B(p,q)]S(p)^{-1} - S(q)^{-1}[1-B(p,q)]\}, \tag{7}$$

wherein $\mathcal{F}^g(k^2)$, $k=p-q$, is the dressing function that appears in the covariant-gauge ghost propagator

$$D^g(k^2,\zeta^2) = -\frac{\mathcal{F}^g(k^2,\zeta^2)}{k^2}, \tag{8}$$

and $B(p,q)$ is the renormalized ghost-quark scattering kernel. At one-loop order on the domain in which perturbation theory is a valid tool

$$\mathcal{F}^g(k^2,\zeta^2) = \left[\frac{\alpha(k^2)}{\alpha(\zeta^2)}\right]^{\gamma_g/\beta_1}, \tag{9}$$

with the anomalous dimensions $\gamma_g=-(3/8)N_c$ in Landau gauge, which we use throughout, and $\beta_1=-(11/6)N_c+(1/3)N_f$, where N_f is the number of active quark flavors. This result may be summarized as $\mathcal{F}^g(k^2)\approx 1$ on the perturbative domain, up to $\ln p^2/\Lambda^2_{\rm QCD}$-corrections. In a similar sense, $B(p,q)\approx 0$ in Landau gauge on this domain.[2]

Equation (7) is a Slavnov-Taylor identity. It is an analogue of the Ward-Takahashi identity that applies to the fermion-photon vertex, which entails that in the vertex describing the coupling of a photon to a dressed-quark:

$$\hat{\Gamma}^\gamma_1(p,p) = A(p^2,\zeta^2), \tag{10}$$

$$\hat{\Gamma}^\gamma_2(p,p) = 2\frac{d}{dp^2}A(p^2,\zeta^2), \tag{11}$$

$$\hat{\Gamma}^\gamma_3(p,p) = 2\frac{d}{dp^2}B(p^2,\zeta^2). \tag{12}$$

Appreciating this nontrivial structure of the dressed-quark-photon vertex has been crucial in describing the electromagnetic properties of mesons [37,38].

The similarity between the Slavnov-Taylor and Ward-Takahashi identities has immediate, important consequences. For example, if the result

[2](An even closer analogy is a kindred result for $Z(p^2)$ in Eq. (2); viz., in Landau gauge $[1-Z(p^2,\zeta^2)]\equiv 0$ at one loop in perturbation theory and hence, on the perturbative domain, corrections to this result are modulated by $\ln\ln p^2/\Lambda^2_{\rm QCD}$. This very slow evolution is exhibited, e.g., in the numerical results of Ref. [19].)

$$0 < \mathcal{F}^g(k^2)[1 - B(p,q)], \tag{13}$$

also prevails on the nonperturbative domain then, because of the known behavior of the dressed-quark propagator, Eq. (13) is sufficient grounds for Eq. (7) to forecast that in the renormalized dressed-quark-gluon vertex $1 < \hat{\Gamma}_1(p,p)$ at infrared spacelike momenta. This result, an echo of Eq. (10), signals that the complete kernel in the DSE satisfied by $\Gamma^a_\mu(p,q)$ is attractive.

B. Vertex in the gap equation

The ability to use the gap equation as the basis for robust statements about DCSB rests on the existence of a systematic, nonperturbative and chiral symmetry preserving truncation scheme. One such scheme, introduced in Ref. [29], may be described as a dressed-loop expansion of the quark-gluon vertex wherever it appears in the half-amputated dressed-quark-antiquark (or -quark-quark) scattering matrix: S^2K, a renormalization-group invariant, where K is the dressed-quark-antiquark (or -quark-quark) scattering kernel. Thereafter, all n-point functions involved in connecting two particular quark-gluon vertices are *fully dressed*.

The effect of this truncation in the gap equation, Eq. (1), is realized through the following representation of the dressed-quark-gluon vertex [30]

$$Z_1\Gamma_\mu(k,p) = \gamma_\mu + \mathcal{L}_2^-(k,p) + \mathcal{L}_2^+(k,p) + [\ldots], \tag{14}$$

with

$$\mathcal{L}_2^-(k,p) = \frac{1}{2N_c}\int_\ell^\Lambda g^2 D_{\rho\sigma}(p-\ell)\,\gamma_\rho S(\ell+k-p)\,\gamma_\mu S(\ell)\,\gamma_\sigma, \tag{15}$$

$$\mathcal{L}_2^+(k,p) = \frac{N_c}{2}\int_\ell^\Lambda g^2 D_{\sigma'\sigma}(\ell) D_{\tau'\tau}(\ell+k-p) \times \gamma_{\tau'} S(p-\ell)\,\gamma_{\sigma'}\Gamma^{3g}_{\sigma\tau\mu}(\ell,-k,k-p), \tag{16}$$

wherein Γ^{3g} is the dressed-three-gluon vertex. The lowest order contribution to each term written explicitly is $O(g^2)$. The ellipsis in Eq. (14) represents terms whose leading contribution is $O(g^4)$; e.g., crossed-box and two-rung dressed-gluon ladder diagrams, and also terms of higher leading-order.

The $\mathcal{L}_2^-$ term in Eq. (14) only differs from a kindred term in QED by the color factor. However, that factor is significant because it flips the sign of the interaction in this channel with respect to QED; i.e., since

$$l^a l^b l^a = \left\{\frac{1}{2}C_2(G) - C_2(R)\right\} l^b = \frac{1}{2N_c} l^b$$

$$\text{cf. } l^a \mathbf{1}_c l^a = -C_2(R)\mathbf{1}_c = -\frac{N_c^2-1}{2N_c}\mathbf{1}_c, \tag{17}$$

then single gluon exchange between a quark and antiquark is repulsive in the color-octet channel. Attraction in the octet channel is provided by the $\mathcal{L}_2^+$ term in Eq. (14), which involves the three-gluon vertex. These observations emphasize that Eq. (7) cannot be satisfied if the contribution from the three gluon vertex is neglected because the Slavnov-Taylor identity signals unambiguously that on the perturbative domain there is net attraction in the octet channel.

It is apparent, too, that the term involving the three gluon vertex is numerically amplified by a factor of N_c^2 cf. the $\mathcal{L}_2^-$ (Abelian-like) vertex correction. Hence, if the integrals are of similar magnitude then the N_c^2-enhanced three-gluon term must dominate in the octet channel. This expectation is borne out by the one-loop perturbative calculation of the two integrals exhibited in Eqs. (15) and (16) and, moreover, the sum of both terms is precisely that combination necessary to satisfy the Slavnov-Taylor identity at this order [39].

C. Vertex model

In illustrating features of the DSE truncation scheme introduced in Ref. [29] in connection, for example, with DCSB, confinement and bound state structure, Ref. [30] employed a dressed-quark-gluon vertex obtained by resumming a subclass of diagrams based on $\mathcal{L}_2^-$ alone; namely, the vertex obtained as a solution of

$$\Gamma^-_\mu(k_+,k_-) = Z_1^{-1}\gamma_\mu + \frac{1}{2N_c}\int_\ell^\Lambda g^2 D_{\rho\sigma}(p-\ell) \times \gamma_\rho S(\ell_+)\Gamma^-_\mu(\ell_+,\ell_-)S(\ell_-)\gamma_\sigma. \tag{18}$$

It was acknowledged that this subclass of diagrams is $1/N_c$-suppressed but, in the absence of nonperturbative information about $\mathcal{L}_2^+$ in general, and the dressed-three-gluon vertex in particular, this limitation was accepted.

Herein we explore a model that qualitatively ameliorates this defect while preserving characteristics that make calculations tractable and results transparent; viz., in Eq. (14) we write

$$\mathcal{L}_2^- + \mathcal{L}_2^+ \approx \mathcal{L}_2^{\mathcal{C}}, \tag{19}$$

where

$$\mathcal{L}_2^{\mathcal{C}}(k,p) := -\mathcal{C}C_2(R)\int_\ell^\Lambda g^2 D_{\rho\sigma}(p-\ell) \times \gamma_\rho S(\ell+k-p)\,\gamma_\mu S(\ell)\,\gamma_\sigma, \tag{20}$$

and work with the vertex obtained as the solution of

$$\Gamma^{\mathcal{C}}_\mu(k_+,k_-) = Z_1^{-1}\gamma_\mu - \mathcal{C}C_2(R)\int_\ell^\Lambda g^2 D_{\rho\sigma}(p-\ell) \times \gamma_\rho S(\ell_+)\Gamma^{\mathcal{C}}_\mu(\ell_+,\ell_-)S(\ell_-)\gamma_\sigma. \tag{21}$$

To explain this model we remark that the parameter $\mathcal{C}$ is a global coupling strength modifier. (NB. The value $\mathcal{C} = -(1/8)$ reproduces the vertex resummed in Ref. [30].) It is introduced so that our *Ansatz* may *mimic* the effects of attraction in the color-octet channel without specifying a form for the three-gluon vertex. This expedient will give a faithful model so long as the integrals over the momentum depen-

dence of $\mathcal{L}_2^-$ and $\mathcal{L}_2^+$ that appear in our calculations are not too dissimilar. This is plausible because: They are both one-loop integrals projected onto the same Dirac and Lorentz structure and hence are pointwise similar at this order in perturbation theory; and their direct sum must conspire to give the simple momentum dependence in Eq. (7). Moreover, as we shall demonstrate, the model has material illustrative capacity and that alone is sufficient justification for proceeding.

D. Interaction model

A simplification, important to our further analysis, is a confining model of the dressed-gluon interaction in Eq. (21). We use [31]

$$\mathcal{D}_{\mu\nu}(k) := g^2 D_{\mu\nu}(k) = \left(\delta_{\mu\nu} - \frac{k_\mu k_\nu}{k^2}\right)(2\pi)^4 \mathcal{G}^2 \delta^4(k). \quad (22)$$

The constant $\mathcal{G}$ sets the model's mass-scale and henceforth we mainly set $\mathcal{G}=1$ so that all mass-dimensioned quantities are measured in units of $\mathcal{G}$. Furthermore, since the model is ultraviolet-finite, we will usually remove the regularization mass-scale to infinity and set the renormalization constants equal to one.

The model defined by Eq. (22) is a precursor to an efficacious class of models that employ a renormalization-group-improved effective interaction and whose contemporary application is reviewed in Refs. [11–13]. It has many features in common with that class and moreover its distinctive momentum-dependence works to advantage in reducing integral equations to algebraic equations that preserve the character of the original. There is a drawback: The simple momentum dependence also leads to some model-dependent artefacts, but they are easily identified and hence not cause for concern.

E. Algebraic vertex and gap equations

If Eq. (22) is used in Eq. (21) then that part of the vertex which acts in the gap equation has no dependence on the total momentum of the quark-antiquark pair; i.e., only $\Gamma^{\mathcal{C}}_\mu(p) := \Gamma^{\mathcal{C}}_\mu(p,p)$ contributes. In this case just the terms written explicitly in Eq. (6) are supported in the dressed vertex, which can be expressed

$$\Gamma^{\mathcal{C}}_\mu(p) = \gamma_\mu \alpha^{\mathcal{C}}_1(p^2) + \gamma\cdot p\, p_\mu \alpha^{\mathcal{C}}_2(p^2) - i p_\mu \alpha^{\mathcal{C}}_3(p^2). \quad (23)$$

Hence we obtain information about all the amplitudes that survive when the vertex is evaluated at zero gluon momentum. The vertex equation is

$$\Gamma^{\mathcal{C}}_\mu(p) = \gamma_\mu - \mathcal{C}\gamma_\rho S(p)\Gamma^{\mathcal{C}}_\mu(p) S(p)\gamma_\rho, \quad (24)$$

where we have used $C_2(R)=4/3$ for $N_c=3$. Equation (24) possesses the solution

$$\Gamma^{\mathcal{C}}_\mu(p) = \sum_{i=0}^{\infty} \Gamma^{\mathcal{C}}_{\mu,i}(p) \quad (25)$$

$$= \sum_{i=0}^{\infty} [\gamma_\mu \alpha^{\mathcal{C}}_{1,i}(p^2) + \gamma\cdot p\, p_\mu \alpha^{\mathcal{C}}_{2,i}(p^2) - i p_\mu \alpha^{\mathcal{C}}_{3,i}(p^2)], \quad (26)$$

where $\Gamma^{\mathcal{C}}_{\mu,i}(p)$ satisfies a recursion relation

$$\Gamma^{\mathcal{C}}_{\rho,i+1}(p) = -\mathcal{C}\gamma_\mu S(p)\Gamma^{\mathcal{C}}_{\rho,i}(p) S(p)\gamma_\mu, \quad (27)$$

with $\Gamma^{\mathcal{C}}_{\mu,i=0}=\gamma_\mu$, the bare vertex, so that $\alpha^{\mathcal{C}}_{1,0}=1$, $\alpha^{\mathcal{C}}_{2,0}=0=\alpha^{\mathcal{C}}_{3,0}$. It follows that ($\Delta(s)=sA^2(s)+B^2(s)$):

$$\alpha^{\mathcal{C}}_1 = \frac{\Delta}{\Delta - 2\mathcal{C}}, \quad (28)$$

$$\alpha^{\mathcal{C}}_2 = -\frac{4\mathcal{C}A^2}{\Delta^2 + 2\mathcal{C}(B^2 - sA^2) - 8\mathcal{C}^2} \frac{(\Delta - 4\mathcal{C})}{(\Delta - 2\mathcal{C})}, \quad (29)$$

$$\alpha^{\mathcal{C}}_3 = -\frac{8\mathcal{C}AB}{\Delta^2 + 2\mathcal{C}(B^2 - sA^2) - 8\mathcal{C}^2}. \quad (30)$$

It is evident that the momentum dependence of the vertex is completely determined by that of the dressed-quark propagator whose behavior, however, the vertex itself influences because it appears in the gap equation. Subject to Eq. (23), that gap equation expresses two coupled algebraic equations:

$$A(s) = 1 + \frac{1}{\Delta(s)}[A(2\alpha^{\mathcal{C}}_1 - s\alpha^{\mathcal{C}}_2) - B\alpha^{\mathcal{C}}_3], \quad (31)$$

$$B(s) = m + \frac{1}{\Delta(s)}[B(4\alpha^{\mathcal{C}}_1 + s\alpha^{\mathcal{C}}_2) - sA\alpha^{\mathcal{C}}_3]. \quad (32)$$

The dressed-quark propagator and -quark-gluon vertex follow from the solution of these equations, which is generally obtained numerically.

In the chiral limit, which here is simply implemented by setting $m=0$, a realization of chiral symmetry in the Wigner-Weyl mode is always possible: It corresponds to the $B\equiv 0$ solution of the gap equation. However, since the phenomena of QCD are built on a Nambu-Goldstone realization of chiral symmetry, we do not consider the Wigner-Weyl mode any further. Its characterization can be achieved in a straightforward manner by adapting the analysis of Ref. [30] to our improved vertex model.

III. PROPAGATOR AND VERTEX SOLUTIONS

A. Algebraic results

At this point some observations are useful in order to establish a context for our subsequent results. To begin we explore the ultraviolet behavior of the model. It is ultraviolet finite and hence at large spacelike momenta, $s \gg 1$ (in units of $\mathcal{G}^2$)

$$A(s) \approx 1 + \frac{a_1}{s}, \quad B(s) \approx m + \frac{b_1}{s}, \quad (33)$$

with m the model's finite current-quark mass. The model is useful because these results persist in asymptotically free theories, up to $\ln p^2/\Lambda^2_{\rm QCD}$-corrections. With this behavior it follows from Eqs. (28)–(33) that:

$$\alpha^{\mathcal{C}}_1(s) \approx 1 + \frac{2\mathcal{C}}{s}, \quad (34)$$

$$\alpha_2^{\mathcal{C}}(s) \approx -\frac{4\mathcal{C}}{s^2}, \quad \alpha_3^{\mathcal{C}}(s) \approx -m\frac{8\mathcal{C}}{s^2}, \tag{35}$$

and these results, in turn, mean that in the ultraviolet the behavior of the massive dressed-quark propagator is determined by the α_1 term in the vertex, so that

$$\underline{a}_1 = 2, \underline{b}_1 = 4m. \tag{36}$$

The expansion of $\alpha_1(s)$ around $1/s=0$ reported in Eq. (34) is the same as that which arises in QCD, apart from the usual $\ln(s/\Lambda_{\rm QCD}^2)$-corrections. However, the leading terms in $\alpha_{2,3}$ are different: On the perturbative domain in QCD these functions both begin with a term of order $(1/s)[\ln(s/\Lambda_{\rm QCD}^2)]^d$, with d some combination of anomalous dimensions. The reason for the mismatch is readily understood. At one-loop order in QCD

$$B(p^2) = \hat{m}\left[\tfrac{1}{2}\ln(p^2/\Lambda_{\rm QCD}^2)\right]^{\gamma_1^m/\beta_1}, \tag{37}$$

with $\hat{m}$ the renormalization point invariant current-quark mass and $\gamma_1^m = (3/2)C_2(R)$. (This makes explicit the logarithmic correction to the leading term in Eq. (33).) For the purpose of this explanation then, on the perturbative domain, with $\mathcal{F}^g(k^2)\approx 1$ and $B(p,q)\approx 0$, the Slavnov-Taylor identity, Eq. (7), is approximately equivalent to the Ward-Takahashi identity. Hence, via Eq. (12)

$$\alpha_3(s) \approx \frac{\hat{m}}{s}\frac{\gamma_1^m}{\beta_1}\left[\frac{1}{2}\ln(p^2/\Lambda_{\rm QCD}^2)\right]^{\gamma_1^m/\beta_1 - 1}. \tag{38}$$

It is thus evident that in QCD, even though they are not themselves divergent, the leading order terms in both $\alpha_{2,3}$ are induced by the momentum-dependent renormalization of elements contributing to their evaluation. Such terms are naturally missing in our ultraviolet finite model. Hence the absence of $1/s$ terms in Eq. (35) is a readily identifiable model artefact.

We note that for $\mathcal{C}>0$, $(\alpha_1^{\mathcal{C}}-1)$ is necessarily positive on the perturbative domain and $\alpha_{2,3}^{\mathcal{C}}$ are negative. These results are also true in QCD ($\alpha_1^{\mathcal{C}}>1$ up to logarithmic corrections). It would be exceptional if these statements were not also true on the nonperturbative domain.

We now turn to the infrared and focus on $s=0$ but consider $0<m\ll 1$, in which case

$$A(s=0,m) \approx a_0^0 + a_0^1 m, \quad B(s=0,m) \approx b_0^0 + b_0^1 m. \tag{39}$$

Upon insertion of these expressions into the gap equation one obtains

$$a_0^0 = 2\frac{2+3\mathcal{C}}{2+\mathcal{C}}, \quad a_0^1 = -\sqrt{2}\frac{4+20\mathcal{C}+15\mathcal{C}^2}{(2+\mathcal{C})^{5/2}}, \tag{40}$$

$$b_0^0 = \sqrt{4+2C}, \quad b_0^1 = \frac{2}{(b_0^0)^2} = \frac{1}{2+\mathcal{C}}; \tag{41}$$

viz., results which show that in the neighborhood of $s=0$ and with attraction in the color-octet channel, $A(s)$ decreases with increasing current-quark mass while $B(s)$ increases. At this order the mass function is

$$M(s=0,m) = \frac{B(0,m)}{A(0,m)} = \mu_0^0 + \mu_0^1 m, \tag{42}$$

with

$$\mu_0^0 = \frac{b_0^0}{a_0^0} = \frac{\sqrt{2}(2+\mathcal{C})^{3/2}}{4+6\mathcal{C}}, \tag{43}$$

$$\mu_0^1 = \frac{b_0^1}{a_0^0} - \frac{b_0^0 a_0^1}{(a_0^0)^2} = \frac{6+23\mathcal{C}+15\mathcal{C}^2}{2(2+3\mathcal{C})^2}. \tag{44}$$

For $\mathcal{C}>-(1/3)$ the mass function also increases with rising m. These patterns of evolution are observed in simulations of lattice-QCD [27].

The infrared behavior of the dressed-quark-gluon vertex follows via Eqs. (28)–(30); using which one finds

$$\alpha_i^{\mathcal{C}}(s=0,m) \approx \mathrm{a}_{i,0}^{\mathcal{C}} + \mathrm{a}_{i,1}^{\mathcal{C}} m, \quad i=1,2,3, \tag{45}$$

$$\mathrm{a}_{1,0}^{\mathcal{C}} = 1 + \frac{\mathcal{C}}{2}, \quad \mathrm{a}_{1,1}^{\mathcal{C}} = -\frac{1}{\sqrt{8}}\frac{\mathcal{C}}{\sqrt{2+\mathcal{C}}}, \tag{46}$$

$$\mathrm{a}_{2,0}^{\mathcal{C}} = -\frac{\mathcal{C}(2-\mathcal{C})(2+3\mathcal{C})}{(2+\mathcal{C})^2}, \tag{47}$$

$$\mathrm{a}_{2,1}^{\mathcal{C}} = \frac{2\sqrt{2}\mathcal{C}(8+20\mathcal{C}+2\mathcal{C}^2-9\mathcal{C}^3)}{(2+\mathcal{C})^{7/2}}, \tag{48}$$

$$\mathrm{a}_{3,0}^{\mathcal{C}} = -\frac{\sqrt{8\mathcal{C}}}{\sqrt{2+\mathcal{C}}}, \quad \mathrm{a}_{3,1}^{\mathcal{C}} = \frac{2\mathcal{C}(5+6\mathcal{C})}{(2+\mathcal{C})^2}. \tag{49}$$

These algebraic formulas show clearly the effect on the dressed-quark-gluon vertex of attraction in the projection of the quark-antiquark scattering kernel onto the color-octet channel. Attraction causes $\hat{\Gamma}_1(p,p)$ to be enhanced in the infrared cf. the bare vertex; and it drives $\hat{\Gamma}_{2,3}(p,p)$ to magnified, negative values. These results also signal that attraction ensures that a current-quark mass acts to reduce the vertex function in magnitude.

B. Numerical results

In choosing a value for C we elect to be guided by results from quenched lattice-QCD simulations of the dressed-quark propagator [27] and dressed-quark gluon vertex [40]. We focus on a current-quark mass common to both simulations; namely, 60 MeV, at which value the lattice dressed-quark propagator has [28]: $Z_{\rm qu}(0)\approx 0.7$, $M_{\rm qu}(0)\approx 0.42$. Then, so as to work with dimensionless quantities, we set $m_{60} = 0.06/M_{\rm qu}(0)$ and, using Eqs. (39)–(49), require a least-squares fit to[3]

$$A(m_{60}) = 1.4, \tag{50}$$

[3](There is a confusion of positive and negative signs in Ref. [40] concerning λ_2, λ_3, as defined therein. Our signs are correct. With the conventions expressed in Eq. (23): $4\lambda_2 = -\alpha_2$ and $2\lambda_3 = \alpha_3$.)

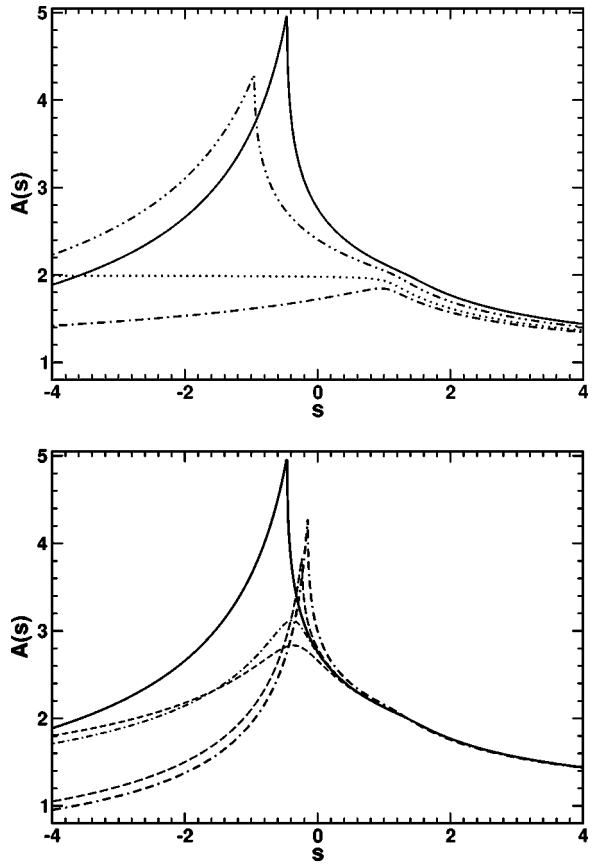

FIG. 1. *Upper panel* – $\mathcal{C}$-dependence of $A(s)$. For all curves $m=0.015$. Solid line: $\mathcal{C}=\overline{\mathcal{C}}=0.51$; dash-dot-dot line: $\mathcal{C}=1/4$; dotted line: $\mathcal{C}=0$; and dash-dot curve: $\mathcal{C}=-1/8$. *Lower panel*–Truncation-dependence of $A(s)$, $\mathcal{C}=\overline{\mathcal{C}}$. Solid line: complete solution; dash-dash-dot line - result obtained with only the $i=0,1$ terms retained in Eq. (25), the one-loop corrected vertex; short-dash line - two-loop corrected; long-dash line - three-loop corrected; and short-dash-dot line: four-loop corrected. In this and subsequent figures, unless otherwise noted, dimensioned quantities are measured in units of $\mathcal{G}$ in Eq. (22). A fit to meson observables requires $\mathcal{G}=0.69$ GeV and hence $m=0.015$ corresponds to 10 MeV.

$$\alpha_1^{\mathcal{C}}(0,m_{60}) = 2.1, \tag{51}$$

$$-M(0,m_{60})^2\alpha_2^{\mathcal{C}}(0,m_{60}) = 7.1, \tag{52}$$

$$-M(0,m_{60})\alpha_3^{\mathcal{C}}(0,m_{60}) = 1.0. \tag{53}$$

This procedure yields

$$C = \overline{C} = 0.51 \tag{54}$$

with an average relative error $\overline{r}=25\%$ and standard deviation $\sigma_r=70\%$. We note that for $\mathcal{C}=0.6$: $\overline{r}=21\%$, $\sigma_r=72\%$, while for $\mathcal{C}=0.4$: $\overline{r}=31\%$, $\sigma_r=67\%$. If one omits Eq. (52) from the fitting requirements then $\overline{\mathcal{C}}=0.49$ with $\overline{r}=2.5\%$ and $\sigma_r=63\%$. It is evident that competing requirements bound the amount of attraction necessary in the kernel. We can now illustrate the results for the dressed-quark propagator and dressed-quark-gluon vertex.

A comparison of the curves in the upper panel of Fig.1 shows clearly that the presence of net attraction in the color-octet quark-antiquark scattering kernel uniformly increases the magnitude of $A(p^2)$ at all momenta. This effect is pronounced at infrared spacelike momenta and particularly on the timelike domain, $s<0$. In this and the following figures $\mathcal{C}=0$ corresponds to the rainbow-ladder DSE truncation; i.e., the leading order term of the truncation scheme introduced in Ref. [29].

In the lower panel one sees that on the spacelike domain, $s>0$, the one-, two-, three- and four-loop corrected vertices yield a result for $A(p^2)$ that is little different from that produced by the completely resummed vertex. However, that is not true on the timelike domain, whereupon confinement is expressed and hence nonperturbative effects become important. In our model confinement is realized via the absence of a particle-like singularity in the dressed-quark propagator [3]. The cusp displayed by $A(p^2)$ in the timelike domain is one manifestation of this feature. The figure shows that convergence to the solution obtained with the completely resummed vertex proceeds via two routes: One followed by solutions obtained with an odd number of loop corrections to the vertex; and another by those obtained using a vertex with an even number of corrections. This effect is absent with net repulsion in the color-octet projection of the quark-antiquark scattering kernel.

We remark that $A(p^2)$ evolves slowly with the current-quark mass when that mass is significantly smaller than the model's mass-scale. However, when the current-quark mass becomes commensurate with or exceeds that mass-scale, it acts to very effectively dampen this function's momentum dependence so that $A(p^2)\approx 1$. This is also true in QCD.

We plot the dressed-quark mass function in Fig. 2. The existence of a nontrivial solution in the chiral limit is the realization of DCSB, in our model and QCD. For current-quark masses less than the model's mass-scale, $\mathcal{G}$, the dynamically generated mass determines the scale of observables. However, for $m\gtrsim\mathcal{G}$, this explicit chiral symmetry breaking mass-scale overwhelms that generated dynamically and enforces $M(p^2)\approx m$. This is the behavior of the b-quark mass function in QCD [32].

From a comparison of the rainbow-ladder result, $\mathcal{C}=0$, in the lower panel with the $\mathcal{C}=-1/8$ and $\overline{\mathcal{C}}=0.51$ results, it is apparent that vertex dressing driven by net attraction in the color-octet scattering kernel reduces the magnitude of the mass function at infrared momenta, a trend which is reversed for spacelike momenta $s\gtrsim\mathcal{G}$.[4] This effect has an impact on the magnitude of the vacuum quark condensate. For example, the mapping of Eq. (3) into our model is

$$-\langle\overline{q}q\rangle^0 = \frac{3}{4\pi^2}\int_0^{s_0} ds\; s\frac{Z(s)M(s)}{s+M(s)^2}, \tag{55}$$

where s_0 is the spacelike point at which the model's mass function vanishes in the chiral limit, and we find

[4](This pattern of behavior is familiar from explorations [20,22] of the effect in the gap equation of vertex Ansätze [14,41]; i.e., vertex models whose diagrammatic content is unknown but which exhibit properties in common with our calculated $C>0$ result.)

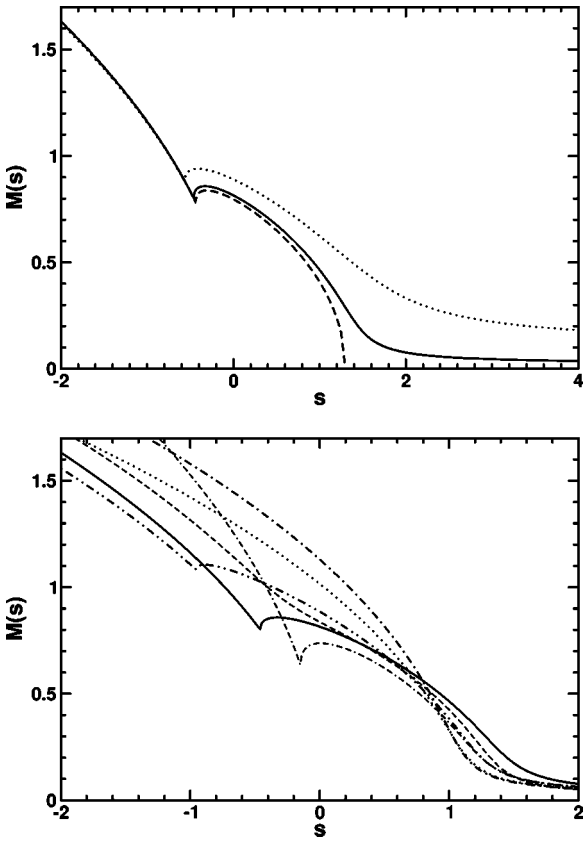

FIG. 2. *Upper panel* – Current-quark-mass-dependence of the dressed-quark mass function. For all curves $\mathcal{C}=\bar{\mathcal{C}}=0.51$. Dotted line: $m=m_{60}$; solid line: $m=0.015$; dashed line: chiral limit, $m=0$. *Lower panel*–$\mathcal{C}$-dependence of $M(s)$. For all curves $m=0.015$. Solid line: $\mathcal{C}=\bar{\mathcal{C}}=0.51$; dash-dot-dot line: $\mathcal{C}=1/4$; dotted line: $\mathcal{C}=0$; and dash-dot curve: $\mathcal{C}=-1/8$. In addition, for $\mathcal{C}=0.51$: dash-dash-dot line - $M(s)$ obtained with one-loop corrected vertex; and short-dash line - with two-loop-corrected vertex.

$$-\langle\overline{q}q\rangle^0_{\mathcal{C}=\bar{\mathcal{C}}}=(0.231\mathcal{G})^3=(0.16\ \mathrm{GeV})^3, \tag{56}$$

with $\mathcal{G}=0.69$ GeV. The rainbow-ladder result is $-\langle\overline{q}q\rangle^0_{\mathcal{C}=0}=\mathcal{G}^3/(10\pi^2)=(0.15\ \mathrm{GeV})^3$ so that

$$\frac{\langle\overline{q}q\rangle^0_{\mathcal{C}=0}}{\langle\overline{q}q\rangle^0_{\mathcal{C}=\bar{\mathcal{C}}}}=0.82. \tag{57}$$

This ratio drops to 0.50 when $\mathcal{C}=1.0$ is used to calculate the denominator.

It is thus evident that with attraction in the scattering kernel and at a common mass-scale, the condensate is significantly larger than that produced by a ladder vertex owing to an expansion of the domain upon which the dressed-quark mass function has nonzero support.

It is natural to ask for the pattern of behavior in the presence of repulsion. In this case Fig. 2 indicates that with $\mathcal{C}=-1/8$ the value of the mass function is enhanced at $s=0$. The magnitude of the mass function grows larger still with a further decrease in $\mathcal{C}$ and its domain of nonzero support expands. Therefore here, too, the condensate is larger than with the ladder vertex; e.g.,

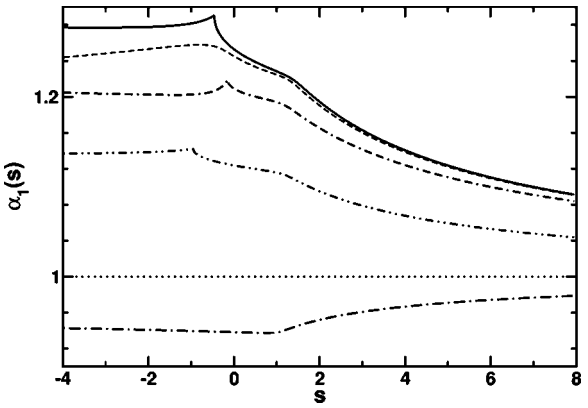

FIG. 3. $\mathcal{C}$-dependence of $\alpha_1^{\mathcal{C}}(s)$ in Eq. (23). For all curves $m=0.015$. Solid line: $\mathcal{C}=\bar{\mathcal{C}}=0.51$; dash-dot-dot line: $\mathcal{C}=1/4$; dotted line: $\mathcal{C}=0$; and dash-dot curve: $\mathcal{C}=-1/8$. In addition, for $\mathcal{C}=0.51$: dash-dash-dot line - one-loop corrected $\alpha_1(s)$; and short-dash line - two-loop-corrected result.

$$\frac{\langle\overline{q}q\rangle^0_{C=0}}{\langle\overline{q}q\rangle^0_{C=-\frac{1}{8}}}=0.92, \tag{58}$$

and the ratio drops to 0.49 when $\mathcal{C}=-3/8$ is used to evaluate the denominator.

The implication of these results is that in general, with a given mass-scale and a common model dressed-gluon interaction, studies employing the rainbow-ladder truncation will materially underestimate the magnitude of DCSB relative to those that employ a well-constrained dressed-quark-gluon vertex. Naturally, in practical phenomenology, alterations of the mass-scale can compensate for this [20].

In Fig. 3 we portray the $\mathcal{C}$-dependence of the scalar function associated with γ_μ in the dressed-quark-gluon vertex, $\alpha_1^{\mathcal{C}}(p^2)$. It is particularly useful here to employ the rainbow-ladder result, $\mathcal{C}=0$, as our reference point because this makes the contrast between the effect of attraction and repulsion in the color-octet quark-antiquark scattering kernel abundantly clear. Attraction uniformly increases the magnitude of $\alpha_1^{\mathcal{C}}(p^2)$, while the opposite outcome is produced by omitting the effect of the three-gluon-vertex in the DSE for the dressed-quark-gluon vertex. We remark that, as with $A(p^2)$, $\alpha_1^{\mathcal{C}}(p^2)$ evolves slowly with the current-quark mass but again, when the current-quark mass becomes commensurate with or exceeds the theory's mass-scale, it acts to very effectively dampen the momentum dependence of this function so that $\alpha_1^{\mathcal{C}}(p^2)\approx 1$. This effect is apparent in the rainbow vertex model employed in Ref. [28] to explain quenched-QCD lattice data.

Figure 4 illustrates the $\mathcal{C}$-dependence of $\alpha_2^{\mathcal{C}}(p^2)$, the scalar function modulating the sub-leading Dirac vector component of the dressed-quark-gluon vertex. The qualitative features of the completely resummed result for $\alpha_1^{\mathcal{C}}(p^2)$ are also manifest here. However, for this component of the vertex, which is purely dynamical in origin, there is a marked difference at timelike momenta between the result obtained with an odd number of loop corrections in the vertex and that obtained with an even number. We note that the magnitude of this

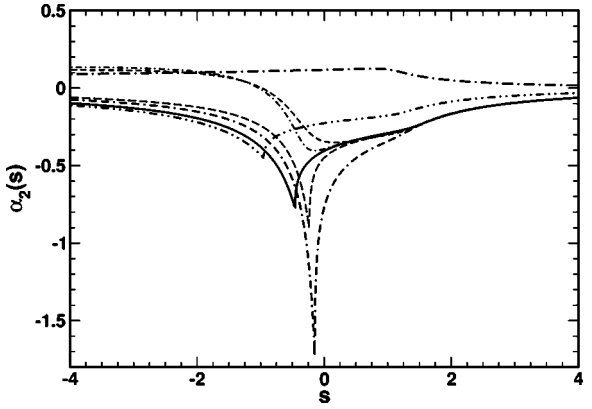

FIG. 4. $\mathcal{C}$-dependence of of $\alpha_2^{\mathcal{C}}(s)$. For all curves $m=0.015$. Solid line: $\mathcal{C}=\bar{\mathcal{C}}=0.51$; dash-dot-dot line: $\mathcal{C}=1/4$; and dash-dot curve: $\mathcal{C}=-1/8$. Moreover, for $\mathcal{C}=0.51$: dash-dash-dot line - one-loop result for $\alpha_2^{\mathcal{C}}(s)$; short-dash line - two-loop result; long-dash line - three-loop; and short-dash-dot line: four-loop. For $\mathcal{C}=0$, $\alpha_2^{\mathcal{C}}(s)\equiv 0$.

function also decreases with increasing current-quark mass.

It is notable that the size of our complete result for $\alpha_2^{\mathcal{C}}(p^2)$ is an order of magnitude smaller than that reported in Ref. [40]. This is an isolated case, however. The calculated magnitudes of the other functions in the dressed-quark propagator and -quark-gluon vertex are commensurate with those obtained in quenched lattice-QCD. We remark in addition that the lattice result is an order of magnitude larger than that obtained with a commonly used vertex *Ansatz* [41]. This discrepancy deserves study in more sophisticated models.

In Fig. 5 we display what might be called the scalar part of the dressed-quark-gluon vertex; viz., $\alpha_3^{\mathcal{C}}(p^2)$. This is the piece of the vertex whose ultraviolet behavior is most sensitive to the current-quark mass. The figure demonstrates that at infrared momenta $\alpha_3^{\mathcal{C}}(p^2)$, too, is materially affected by the scale of DCSB, Eq. (56): at $s=0$ the deviation from its rainbow-truncation value is approximately four times that exhibited by $\alpha_1^{\mathcal{C}}(p^2)$. Hence, this term can be important at infrared and intermediate momenta.

Finally, since they are absent in rainbow truncation, it is illuminating to unfold the different roles played by $\alpha_2^{\mathcal{C}}(s)$ and $\alpha_3^{\mathcal{C}}(s)$ in determining the behavior of the gap equation's self-consistent solution. Some of these effects are elucidated in Fig. 6. The key observation is that $\alpha_3^{\mathcal{C}}(s)$ alone is the source of all coupling between Eqs. (31) and (32) that is not already present in rainbow-ladder truncation: $\alpha_3^{\mathcal{C}}B$ appears in the equation for $A(s)$ and $\alpha_3^{\mathcal{C}}sA$ appears in the equation for $B(s)$. The action of $\alpha_2^{\mathcal{C}}$ is merely to modify the rainbow-ladder coupling strengths.

A consideration of Eqs. (31) and (32) suggests that omitting $\alpha_3^{\mathcal{C}}(s)$ will affect $A(s)$ at infrared momenta but not $B(s)$. That is easily substantiated by repeating the analysis that gave Eqs. (40) and (41), and is apparent in the figure. It will readily be appreciated that neither $\alpha_2^{\mathcal{C}}(s)$ nor $\alpha_3^{\mathcal{C}}(s)$ can affect the deep ultraviolet behavior of the gap equation's solution, Eqs. (33) and (36), because they vanish too rapidly as $1/s \to 0$. This is plain in Fig. 6.

At intermediate spacelike momenta both $\alpha_2^{\mathcal{C}}(s)$ and $\alpha_3^{\mathcal{C}}(s)$ are negative and hence act to magnify $A(s)$ with respect to

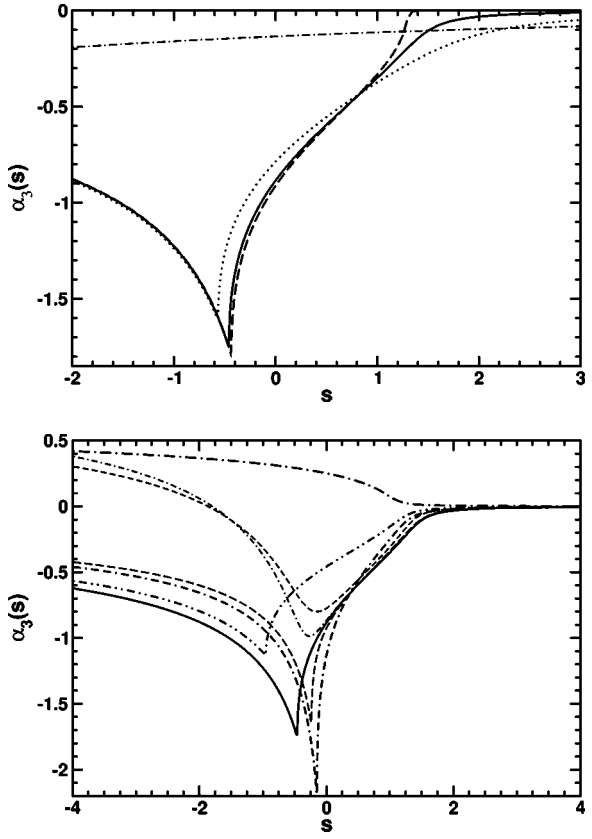

FIG. 5. *Upper panel* – Current-quark-mass-dependence of $\alpha_3^{\mathcal{C}}(s)$. For all curves $\mathcal{C}=\bar{\mathcal{C}}=0.51$. Dash-dot line: $m=2$; dotted line: $m=m_{60}$; solid line: $m=0.015$; dashed line: chiral limit, $m=0$. *Lower panel*–$\mathcal{C}$-dependence of $\alpha_3^{\mathcal{C}}(s)$. For all curves $m=0.015$. Solid line: $\mathcal{C}=\bar{\mathcal{C}}=0.51$; dash-dot-dot line: $\mathcal{C}=1/4$; and dash-dot curve: $\mathcal{C}=-1/8$. Moreover, for $\mathcal{C}=0.51$: dash-dash-dot line - one-loop result for $\alpha_3^{\mathcal{C}}(s)$; short-dash line - two-loop result; long-dash line - three-loop; and short-dash-dot line: four-loop. For $C=0$, $\alpha_3^{\mathcal{C}}(s)\equiv 0$.

the value obtained using a bare vertex. However, they compete in Eq. (32): $\alpha_2^{\mathcal{C}}(s)$ works to diminish $B(s)$ and $\alpha_3^{\mathcal{C}}(s)$ acts to amplify it. Therefore, in the absence of $\alpha_3^{\mathcal{C}}(s)$ one should expect $M(s)=B(s)/A(s)$ to be suppressed at intermediate momenta, and consequently a condensate much reduced in magnitude. Omitting $\alpha_2^{\mathcal{C}}(s)$ should yield the opposite effect. This is precisely the outcome of our numerical studies:

$$\left.\frac{\langle\overline{q}q\rangle^0_{\mathcal{C}=0}}{\langle\overline{q}q\rangle^0_{\mathcal{C}=\bar{\mathcal{C}}}}\right|_{\alpha_3^{\mathcal{C}}\equiv 0} = 1.97; \quad \text{and} \quad \left.\frac{\langle\overline{q}q\rangle^0_{\mathcal{C}=0}}{\langle\overline{q}q\rangle^0_{\mathcal{C}=\bar{\mathcal{C}}}}\right|_{\alpha_2^{\mathcal{C}}\equiv 0} = 0.40. \tag{59}$$

These aspects of our model provide an algebraic illustration of results obtained with more sophisticated *Ansätze*, as apparent from a comparison with, for example, Refs. [20,22].

IV. BETHE-SALPETER EQUATION

The renormalized homogeneous Bethe-Salpeter equation (BSE) for the quark-antiquark channel denoted by M can be compactly expressed as

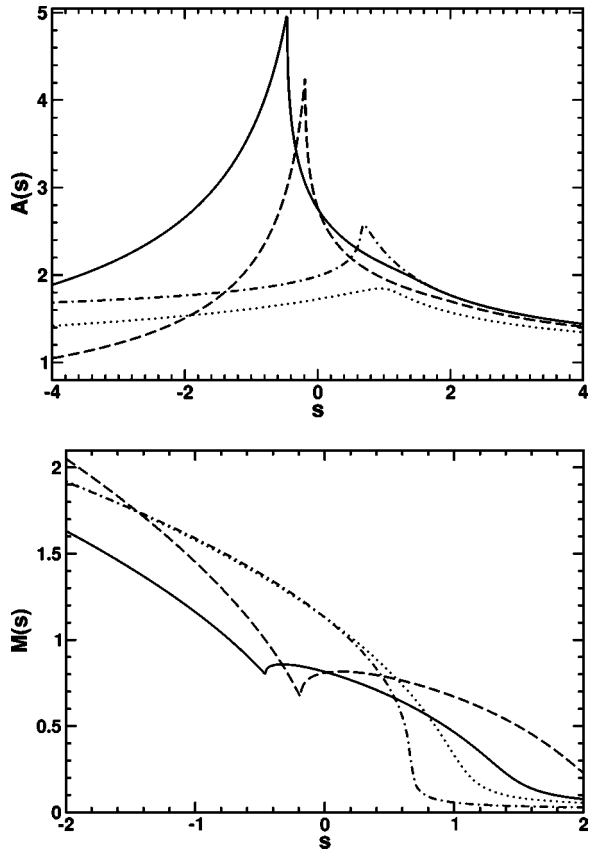

FIG. 6. *Upper panel* – Impact of $\alpha_2^{\mathcal{C}}(s)$ and $\alpha_3^{\mathcal{C}}(s)$ on $A(s)$. For $\mathcal{C}=\bar{\mathcal{C}}$, Eq. (54), solid line: result obtained with both terms present; dashed-line: $\alpha_2^{\mathcal{C}}(s)$omitted; dash-dot line: $\alpha_3^{\mathcal{C}}(s)$ omitted. The dotted line is the result obtained with both terms present in the vertex but $\mathcal{C}=-1/8$. *Lower panel*–Impact of $\alpha_2^{\mathcal{C}}(s)$ and $\alpha_3^{\mathcal{C}}(s)$ on $M(s)$. In all cases $m=0.015$.

$$[\Gamma_M(k;P)]_{EF} = \int_q^\Lambda [K(k,q;P)]_{EF}^{GH} [\chi_M(q;P)]_{GH}, \quad (60)$$

where: k is the relative momentum of the quark-antiquark pair and P is their total momentum; $E,\ldots,H$ represent color, flavor and spinor indices; and

$$\chi_M(k;P) = S(k_+)\Gamma_M(k;P)S(k_-), \quad (61)$$

with $\Gamma_M(q;P)$ the meson's Bethe-Salpeter amplitude. In Eq. (60), K is the fully-amputated dressed-quark-antiquark scattering kernel.

A. Vertex consistent kernel

The preservation of Ward-Takahashi identities in those channels related to hadron observables requires a conspiracy between the dressed-quark-gluon vertex and the Bethe-Salpeter kernel [29,42]. The manner in which these constraints are realized for vertices of the class considered herein was made explicit in Ref. [30]. In that systematic and nonperturbative truncation scheme the rainbow gap equation and ladder Bethe-Salpeter equation represent the lowest-order Ward-Takahashi identity preserving pair. Beyond this, each additional term in the vertex generates a unique collection of terms in K, a subset of which are always nonplanar.

For any dressed-quark-gluon vertex in the gap equation, which can be represented expressly by an enumerable series of contributions, the Bethe-Salpeter kernel that guarantees the validity of all Ward-Takahashi identities is realized in

$$\Gamma_M(k;P) = \int_q^\Lambda \mathcal{D}_{\mu\nu}(k-q) l^a \gamma_\mu [\chi_M(q;P) l^a \Gamma_\nu(q_-,k_-) + S(q_+)\Lambda^a_{M\nu}(q,k;P)], \quad (62)$$

where

$$\Lambda^a_{M\nu}(q,k;P) = \sum_{n=0}^{\infty} \Lambda^{a;n}_{M\nu}(q,k;P), \quad (63)$$

with herein

$$-\frac{1}{8\mathcal{C}}\Lambda^{a;n}_{M\nu}(\ell,k;P) = \int_q^\Lambda \mathcal{D}_{\rho\sigma}(\ell-q) l^b \gamma_\rho \chi_M(q;P) \times l^a \Gamma^C_{\nu,n-1}(q_-,q_-+k-\ell) S(q_-+k-\ell) l^b \gamma_\sigma + \int_q^\Lambda D_{\rho\sigma}(k-q) l^b \gamma_\rho S(q_+ + \ell - k) \times l^a \Gamma^C_{\nu,n-1}(q_+ + \ell - k, q_+) \chi_M(q;P) l^b \gamma_\sigma + \int_{q'}^\Lambda \mathcal{D}_{\rho\sigma}(\ell - q') l^b \gamma_\rho S(q'_+) \times \Lambda^{a;n-1}_\nu(q', q' + k - \ell; P) \times S(q'_- + k - \ell) l^b \gamma_\sigma. \quad (64)$$

This last equation is a recursion relation, which is to be solved subject to the initial condition $\Lambda^{a;0}_{M\nu} \equiv 0$.

The Bethe-Salpeter amplitude for any meson can be written in the form

$$\Gamma_M(k;P) = I_c \sum_{i=1}^{N_M} \mathcal{G}^i(k;P) f^i_M(k^2, k\cdot P; P^2) = :[\boldsymbol{G}]\, \boldsymbol{f}_M, \quad (65)$$

where $\mathcal{G}^i(k;P)$ are those independent Dirac matrices required to span the space containing the meson under consideration. It then follows upon substitution of this formula that Eq. (64) can be written compactly as:

$$\Lambda^{a;n}_{M\nu} = \{[\mathcal{K}^i_{M\nu}\alpha^C_{i;n-1}] + [\mathcal{L}\Lambda^{a;n-1}_{M\nu}]\}\, \boldsymbol{f}_M. \quad (66)$$

This states that $\Lambda^{a;n}_{M\nu}$ can be considered as a matrix operating in the space spanned by the independent components of the Bethe-Salpeter amplitude, with its Dirac and Lorentz structure projected via the contractions in the BSE. The first term ($\mathcal{K}_M$) in Eq. (66) represents the contribution from the first two integrals on the right-hand side (r.h.s.) of Eq. (64). This is the driving term in the recursion relation. The second term ($\mathcal{L}$) represents the last integral, which enacts the recursion.

B. Solutions of the vertex-consistent meson Bethe-Salpeter equation

1. π-meson

With the model of the dressed-gluon interaction in Eq. (22) the relative momentum between a meson's constituents must vanish. It follows that the general form of the Bethe-Salpeter amplitude for a pseudoscalar meson of equal-mass constituents is ($\hat{P}^2=1$)

$$\Gamma_\pi(P) = \gamma_5[if_1^\pi(P^2) + \gamma\cdot\hat{P} f_2^\pi(P^2)]. \tag{67}$$

To obtain the vertex-consistent BSE one must first determine $\Lambda^{a;1}_{\pi\nu}$. That is obtained by substituting Eq. (67) into the r.h.s. of Eq. (64). Only the first two integrals contribute because of the initial condition and they are actually algebraic expressions when Eq. (22) is used. This gives $\mathcal{K}^i_{\pi\nu}$ in Eq. (66). Explicit calculation shows this to be identically zero, and hence $\Lambda^{a;1}_{\pi\nu}\equiv 0$. Since this is the driving term in the recursion relation then

$$\Lambda^a_{\pi\nu}(k,k;P) \equiv 0. \tag{68}$$

While this result is not accidental [30], it is not a general feature of the vertex-consistent Bethe-Salpeter kernel.

One thus arrives at a particularly simple vertex-consistent BSE for the pion ($Q=P/2$):

$$\Gamma_\pi(P) = -\gamma_\mu S(Q)\Gamma_\pi(P)S(-Q)\Gamma^{\mathcal{C}}_\mu(-Q). \tag{69}$$

Consider the matrices

$$\mathcal{P}_1 = -\frac{i}{4}\gamma_5, \quad \mathcal{P}_2 = \frac{1}{4}\gamma\cdot\hat{P}\gamma_5, \tag{70}$$

which satisfy

$$f_i^\pi(P) = \mathrm{tr}_D\mathcal{P}_i\Gamma_\pi(P). \tag{71}$$

They may be used to rewrite Eq. (69) in the form

$$\boldsymbol{f}_\pi(P) = \mathcal{H}_\pi(P^2)\boldsymbol{f}_\pi(P), \tag{72}$$

wherein $\mathcal{H}_\pi(P^2)$ is a 2×2 matrix

$$\mathcal{H}_\pi(P^2)_{ij} = -\frac{\delta}{\delta f_j^\pi}\mathrm{tr}_D\mathcal{P}_i\gamma_\mu S(Q)\Gamma_\pi(P)S(-Q)\Gamma^{\mathcal{C}}_\mu(-Q). \tag{73}$$

Equation (72) is a matrix eigenvalue problem in which the kernel $\mathcal{H}$ is a function of P^2. This equation has a nontrivial solution if, and only if, at some M^2

$$det[\mathcal{H}_\pi(P^2) - \mathbf{I}]_{P^2+M^2=0} = 0. \tag{74}$$

The value of M for which this characteristic equation is satisfied is the bound state's mass. In the absence of a solution there is no bound state in this channel.

We have solved Eq. (74) for the pion and the results are presented in Table I. That the vertex-consistent Bethe-Salpeter kernel ensures the preservation of the axial-vector Ward-Takahashi identity, and hence guarantees the pion is a Goldstone boson in the chiral limit, is abundantly clear: irrespective of the value of C and the order of the truncation, $m_\pi=0$ for $m=0$. Away from this symmetry-constrained point the results indicate that, with net attraction in the color-octet quark-antiquark scattering kernel, the rainbow-ladder truncation overestimates the mass; i.e., it yields a value greater than that obtained with the fully resummed vertex ($n=\infty$). Moreover, the approach to the exact result for the mass is not monotonic. On the other hand, given two truncations for which solutions exist, characterised by n_1- and n_2-loop insertions, respectively, then

$$|M_H^{n=\infty} - M_H^{n_2}| < |M_H^{n=\infty} - M_H^{n_1}|, \quad n_2 > n_1, \tag{75}$$

viz., correcting the vertex improves the accuracy of the mass estimate.

TABLE I. Calculated π and ρ meson masses, in GeV. ($\mathcal{G}=0.69$ GeV, in which case $m=0.015$ $\mathcal{G}=10$ MeV. In the notation of Ref. [29], this value of $\mathcal{G}$ corresponds to $\eta=1.39$ GeV.) n is the number of loops retained in dressing the quark-gluon vertex, see Eq. (25), and hence the order of the vertex-consistent Bethe-Salpeter kernel. NB. $n=0$ corresponds to the rainbow-ladder truncation, in which case $m_\rho=\sqrt{2}\mathcal{G}$, and that is why this column's results are independent of $\mathcal{C}$.

		$M_H^{n=0}$	$M_H^{n=1}$	$M_H^{n=2}$	$M_H^{n=\infty}$
$\mathcal{C}=-(1/8)$	π, $m=0$	0	0	0	0
	π, $m=0.01$	0.149	0.153	0.154	0.154
	ρ, $m=0$	0.982	1.074	1.089	1.091
	ρ, $m=0.01$	0.997	1.088	1.103	1.105
$\mathcal{C}=(1/4)$	π, $m=0$	0	0	0	0
	π, $m=0.01$	0.149	0.140	0.142	0.142
	ρ, $m=0$	0.982	0.789	0.855	0.842
	ρ, $m=0.01$	0.997	0.806	0.871	0.858
$\mathcal{C}=\bar{\mathcal{C}}=0.51$	π, $m=0$	0	0	0	0
	π, $m=0.01$	0.149	0.132	0.140	0.138
	ρ, $m=0$	0.982	…	0.828	0.754
	ρ, $m=0.01$	0.997	…	0.844	0.770

2. ρ-meson

In our algebraic model the complete form of the Bethe-Salpeter amplitude for a vector meson is

$$\Gamma^\lambda_\rho(P) = \gamma\cdot\boldsymbol{\epsilon}^\lambda(P) f_1^\rho(P^2) + \sigma_{\mu\nu}\boldsymbol{\epsilon}^\lambda_\mu(P)\hat{P}_\nu f_2^\rho(P^2). \tag{76}$$

This expression, which has only two independent functions, is simpler than that allowed by a more sophisticated interaction, wherein there are eight terms. Nevertheless, Eq. (76) retains the amplitudes that are found to be dominant in more sophisticated studies [43]. In Eq. (76), $\{\boldsymbol{\epsilon}^\lambda_\mu(P);\lambda=-1,0,+1\}$ is the polarization four-vector:

$$P\cdot\boldsymbol{\epsilon}^\lambda(P) = 0, \quad \forall\,\lambda; \quad \boldsymbol{\epsilon}^\lambda(P)\cdot\boldsymbol{\epsilon}^{\lambda'}(P) = \delta^{\lambda\lambda'}. \tag{77}$$

The construction of the vertex-consistent ρ-meson BSE for the class of vertices under consideration herein is fully described in Ref. [30]. The pion case illustrates the key modification. Brevity requires that we omit further details. Suffice to say, one arrives via a mechanical procedure at the

characteristic equation for the ρ-meson, which we solved.

The results are presented in Table I. With increasing net attraction in the quark-antiquark scattering kernel the amount by which the rainbow-ladder truncation overestimates the exact mass also increases: With the amount of attraction suggested by lattice data the $n=0$ mass is 27% too large. A related observation is that the bound state's mass decreases as the amount of attraction between its constituents increases. Furthermore, with increasing attraction, even though the fully resummed vertex and consistent kernel always yield a solution, there is no guarantee that a given truncated system supports a bound state: the one-loop corrected vertex and consistent kernel ($n=1$) do not have sufficient binding to support a ρ-meson. This is overcome at the next order of truncation, which yields a mass 9.7% too large. The observation that a given beyond-rainbow-ladder truncation may not support a bound state, even though one is present in the solution of the complete and consistent system, provides a valuable and salutary tip for model building and hadron phenomenology.

Finally, as has often been observed, and independent of the truncation, bound state solutions of gap-equation-consistent BSEs always yield the full amount of π-ρ mass splitting, even in the chiral limit. This splitting is driven by the DCSB mechanism. Its true understanding, therefore, requires a veracious realization of that phenomenon.

3. Dependence on the current-quark mass

In connection with this last observation it is relevant to explore the evolution with current-quark mass of the pseudoscalar and vector meson masses, and of the difference between them. The results for pseudoscalar mesons should be interpreted with the following caveat in mind. In constructing the vertex and kernel we omitted contributions from gluon vacuum polarization diagrams. These contribute only to flavor diagonal meson channels. Hence, for light-quarks in the pseudoscalar channel, wherewith such effects may be important [44,45], our results should be understood to apply only to flavor nonsinglets. In principle, the same is true for light vector mesons. However, experimentally, the ω and ϕ mesons are almost ideally mixed; i.e., the ω exhibits no $\bar{s}s$ content whereas the ϕ is composed almost entirely of this combination. We therefore assume that the vacuum polarization diagrams we have omitted are immaterial in the study of vector mesons. (NB.It is an artefact of Eq. (22) that this model supports neither scalar nor axial-vector meson bound states [30,31].)

We fix the model's current-quark masses via a fit to vector meson masses and the results are presented in Table II. The model we are employing is ultraviolet finite and hence our current-quark masses cannot be directly compared with QCD's current-quark mass-scales. Nevertheless, the values are quantitatively consistent with the pattern of flavour-dependence in the explicit chiral symmetry breaking masses of QCD.

Our calculated results for the current-quark mass-dependence of pseudoscalar and vector meson masses are presented in Fig. 7. In the neighborhood of the chiral limit the vector meson mass is approximately independent of the current-quark mass whereas the pseudoscalar meson mass increases rapidly, according to (in GeV)

TABLE II. Current-quark masses required to reproduce the experimental masses of the vector mesons. The values of m_{η_c}, m_{η_b} are predictions. Experimentally [46], $m_{\eta_c}=2.9797\pm0.000\ 15$ and $m_{\eta_b}=9.30\pm0.03$. NB. $0^-_{s\bar{s}}$ is a fictitious pseudoscalar meson composed of unlike-flavor quarks with mass m_s, which is included for comparison with other nonperturbative studies. All masses are listed in GeV.

$m_{u,d}=0.01$	$m_s=0.166$	$m_c=1.33$	$m_b=4.62$
$m_\rho=0.77$	$m_\phi=1.02$	$m_{J/\psi}=3.10$	$m_{\Upsilon(1S)}=9.46$
$m_\pi=0.14$	$m_{0^-_{s\bar{s}}}=0.63$	$m_{\eta_c}=2.97$	$m_{\eta_b}=9.42$

$$m_{0^-}^2 \approx 1.33m \quad m \ll \mathcal{G}, \tag{78}$$

thereby reproducing the pattern predicted by QCD [8].

With the model's value of the vacuum quark condensate, Eq. (56), this result allows one to infer the chiral-limit value

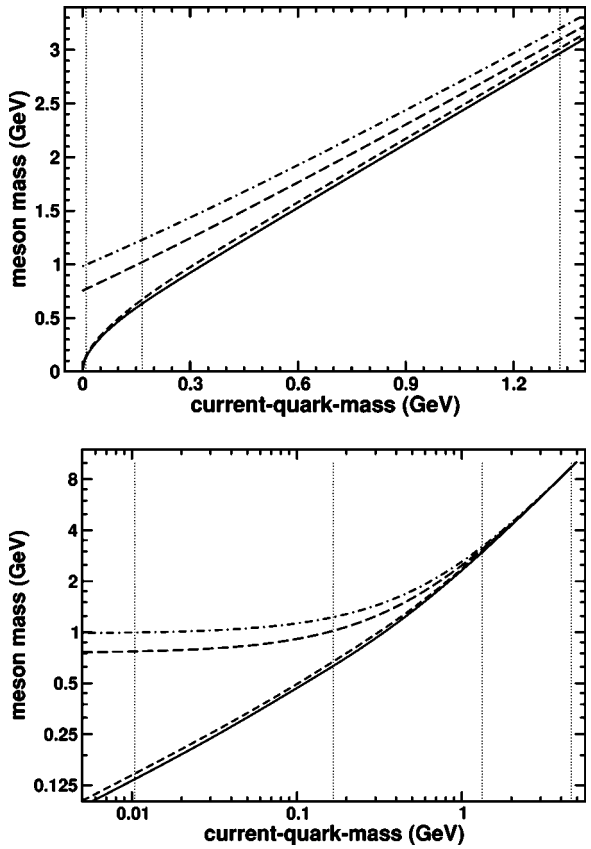

FIG. 7. Evolution of pseudoscalar and vector $q\bar{q}$ meson masses with the current-quark mass. Solid line: pseudoscalar meson trajectory obtained with $\mathcal{C}=\bar{\mathcal{C}}=0.51$, Eq. (54), using the completely resummed dressed-quark-gluon vertex in the gap equation and the vertex-consistent Bethe-Salpeter kernel; short-dash line: this trajectory calculated in rainbow-ladder truncation. Long-dash line: vector meson trajectory obtained with $\bar{\mathcal{C}}$ using the completely resummed vertex and the consistent Bethe-Salpeter kernel; dash-dot line: rainbow-ladder truncation result for this trajectory. The dotted vertical lines mark the current-quark masses in Table II.

of $f_\pi^0 = 0.079$ GeV via the Gell-Mann–Oakes–Renner relation. It is a model artefact that the relative-momentum-dependence of Bethe-Salpeter amplitudes is described by $\delta^4(p)$ and so a direct calculation of this quantity is not realistic. The value is low, as that of the condensate is low, because the model is ultraviolet finite. In QCD the condensate and decay constant are influenced by the high-momentum tails of the dressed-quark propagator and Bethe-Salpeter amplitudes [9,43].

The curvature in the pseudoscalar trajectory persists over a significant domain of current-quark mass. For example, consider two pseudoscalar mesons, one composed of unlike-flavour quarks each with mass $2m_s$ and another composed of such quarks with mass m_s. In this case

$$\frac{m^2_{0^-_{2m_s}}}{m^2_{0^-_{m_s}}} = 2.4, \tag{79}$$

which indicates that the nonlinear evolution exhibited in Eq. (78) is still evident for current-quark masses as large as twice that of the *s*-quark. With this result we reproduce a feature of more sophisticated DSE studies [47–49] and a numerical simulation of quenched lattice-QCD [50].

The mode of behavior just described is overwhelmed when the current-quark mass becomes large: $m \gg \mathcal{G}$. In this limit the vector and pseudoscalar mesons become degenerate, with the mass of the ground state pseudoscalar meson rising monotonically to meet that of the vector meson. In our model

$$\left.\frac{m_{1^-}}{m_{0^-}}\right|_{m=m_c} = 1.04, \tag{80}$$

with a splitting of 130 MeV, and this splitting drops to just 40 MeV at m_b; viz., only 5% of its value in the chiral limit. In addition to the calculated value, the general pattern of our results argues for the mass of the pseudoscalar partner of the $\Upsilon(1S)$ to lie above 9.4 GeV. Indeed, we expect the mass splitting to be less than $m_{J/\psi} - m_{\eta_c}$, not more. (See also; e.g., Ref. [51].)

In Fig. 8 one observes that on a material domain of current-quark masses: $m^2_{1^-} - m^2_{0^-} \approx 0.56$ GeV, an outcome consistent with experiment that is not reproduced in numerical simulations of quenched lattice-QCD [50]. The difference is maximal in the vicinity of m_c, a result which re-emphasises that heavy-quark effective theory is not an appropriate tool for the study of *c*-quarks [32].

Figure 9 is instructive. It shows that with growing current-quark mass the rainbow-ladder truncation provides an increasingly accurate estimate of the ground state vector meson mass. At the *s*-quark mass the relative error is 20% but that has fallen to $<4\%$ at the *c*-quark mass.

Similar statements are true in the valid pseudoscalar channels. In fact, in this case the agreement between the truncated and exact results is always better; e.g., the absolute difference reaches its peak of ≈ 60 MeV at $m \sim 4m_s$ whereat the relative error is only 3%. This behavior is fundamentally because of Goldstone's theorem, which requires that all legitimate truncations preserve the axial-vector Ward-Takahashi identity and hence give a massless pseudoscalar meson in the chiral limit. It is practically useful, too, because it indicates that the parameters of a model meant to be employed in a rainbow-ladder truncation study of hadron observables may reliably be fixed by fitting to the values of quantities calculated in the neighborhood of the chiral limit.

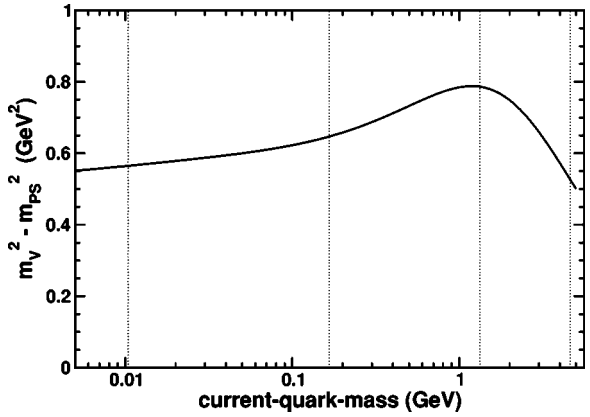

FIG. 8. Evolution with current-quark mass of the difference between the squared-masses of vector and pseudoscalar mesons ($\overline{C} = 0.51$) using the completely resummed dressed-quark-gluon vertex in the gap equation and the vertex-consistent Bethe-Salpeter kernel. The dotted vertical lines mark the current-quark masses in Table II.

The general observation suggested by Fig. 9 is that with increasing current-quark mass the contributions from nonplanar diagrams and vertex corrections are suppressed in both the gap and Bethe-Salpeter equations. Naturally, they must still be included in precision spectroscopic calculations. It will be interesting to reanalyze this evolution in a generalization of our study to mesons composed of constituents with different current-quark masses, and thereby extend and complement the limited such trajectories in Refs. [47,48].

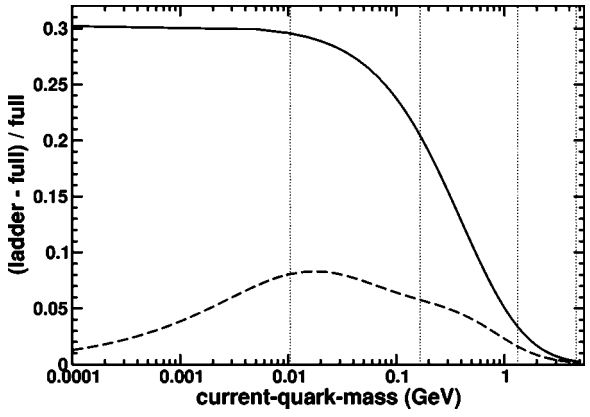

FIG. 9. Evolution with current-quark mass of the relative difference between the meson mass calculated in the rainbow-ladder truncation and the exact value. Solid lines: vector meson trajectories; and dashed-lines; pseudoscalar meson trajectories. The dotted vertical lines mark the current-quark masses in Table II. We used $\overline{C} = 0.51$.

C. Bethe-Salpeter equation for diquarks

Color antitriplet quark-quark correlations (diquarks) have long been a focus of attempts to understand baryon structure [52]. An appreciation of their importance has grown and a modern picture of diquark correlations in baryons is realized through their role in a Poincaré covariant Faddeev equation [4,53–55]. Lorentz scalar and axial-vector correlations are most important.

In rainbow-ladder truncation color-antitriplet diquarks are true bound states [56,57]. (NB. Color sextet diquarks are never bound since even single gluon exchange is repulsive in that channel.) In spite of this, the addition of $\mathcal{L}_2^2(k,p)$, Eq. (15), to the quark-gluon vertex, along with the three terms it generates in the color-antitriplet quark-quark scattering kernel, overwhelms the attraction produced by single gluon exchange and eliminates diquarks from the spectrum [29]. The repulsive effect owing to $\mathcal{L}_2^-(k,p)$ is consummated when the series it generates is fully resummed [30]. With that vertex the characteristic polynomial obtained from the Bethe-Salpeter equation exhibits a pole, which is the antithesis of the zero associated with a bound state.

Herein we have introduced a new element into the consideration of diquarks; namely, our model for the quark-antiquark scattering kernel exhibits attraction, which is a property not possessed by $\mathcal{L}_2^-(k,p)$. The dressed-quarks that appear in the diquark Bethe-Salpeter equation are described by the gap equation elucidated already. However, the manner in which diagrams are combined and resummed in the vertex-consistent color-antitriplet diquark Bethe-Salpeter kernel is different from that which maintains for color singlet mesons. Fortunately, the modifications necessary in the class of *Ansätze* containing our model were elucidated in Ref. [30] and we need only adapt them to our particular case.

Brevity requires that we omit all details and herein it must suffice to say that we examined the behavior of the scalar and axial-vector diquarks' characteristic equations as the parameter $\mathcal{C}$ in Eq. (20) was varied. Our results are summarised in Fig. 10. A value of $\mathcal{C}=0$ implements the rainbow-ladder truncation. In this case, as promised, both scalar and axial-vector diquarks are bound, with $m_{0^+}=1.55$ GeV and $m_{1^+}=1.70$ GeV, in agreement with Ref. [29].

When $\mathcal{C}$ is evolved to negative values (net repulsion in the color-octet projection of the quark-antiquark scattering kernel) the zero in both characteristic equations moves deeper into the timelike region; i.e., the diquark masses increase. This continues briefly until, at $\mathcal{C}_{1^+}^- \approx -0.023 \approx -1/43$, the characteristic equation for the axial-vector diquark no longer has a solution. For the scalar diquark this happens at $\mathcal{C}_{0^+}^- \approx -0.027 \approx -1/37$. It is therefore clear that very little repulsion in the color-octet quark-antiquark scattering kernel is sufficient to prevent the appearance of diquark bound states. (NB. If one considers single-gluon exchange between the quark and antiquark then a value of $\mathcal{C}=-1/8$ is obtained, Eq. (17). This is approximately five-times larger than these critical values, an observation which further elucidates the results in Refs. [29,30].)

The evolution of $\mathcal{C}$ to positive values provides altogether new information and insight. To begin, the bound diquarks

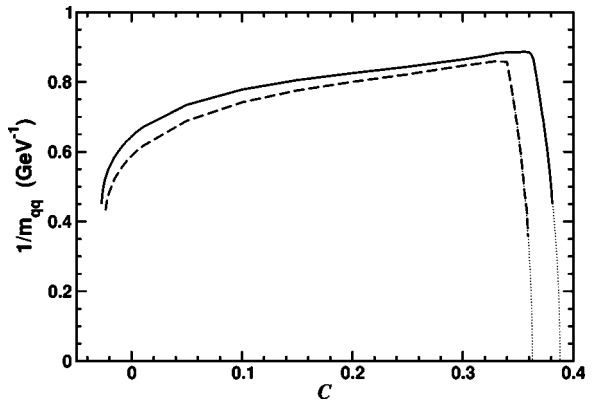

FIG. 10. Evolution of the reciprocal diquark masses, calculated in the chiral limit, with the parameter $\mathcal{C}$: solid line – scalar diquark, dashed line – axial-vector diquark. The dotted lines are explained in connection with Eq. (81). $\mathcal{G}=0.69$ GeV.

that existed in rainbow-ladder truncation survive and their masses decrease continuously with increasing $\mathcal{C}$. Such behavior might have been anticipated on the basis of continuity, and a decrease in a bound state's mass with increasing attraction between its constituents is not unusual. This smooth development continues, for the axial-vector diquark until $\mathcal{C}_{1^+}^+ \approx 0.34$ and for the scalar diquark until $\mathcal{C}_{0^+}^+ \approx 0.36$, at which point it changes dramatically. The masses suddenly begin to increase rapidly and their behavior thereafter is described by

$$\frac{1}{m_{0^+}} = 5.59\sqrt{0.388-\mathcal{C}}, \quad \frac{1}{m_{1^+}} = 5.75\sqrt{0.363-\mathcal{C}}, \quad (81)$$

an evolution represented by the dotted lines in Fig. 10.

The value of $\mathcal{C}$ at which the behavior of the masses changes qualitatively is correlated with the movement of the cusp evident in Figs. 1–5 into the domain that affects the position of the zero in the characteristic polynomials. This means that, with net attraction in the color-octet quark-antiquark scattering channel, the expulsion of diquarks from the bound state spectrum follows immediately upon the active expression of confinement by the dressed-quark propagator in the bound state equation.

There are no bound diquarks in the spectrum obtained with the value of $\mathcal{C}=\overline{\mathcal{C}}$ in Eq. (54) suggested by the lattice data.

V. EPILOGUE

We explored the character of the dressed-quark-gluon vertex and its role in the gap and Bethe-Salpeter equations. Our results are relevant to the mechanism and realization of confinement and dynamical chiral symmetry breaking, and the formation of bound states.

We employed a simple model for the dressed-gluon interaction to build an *Ansatz* for the quark-gluon vertex whose diagrammatic content is expressly enumerable. The model reduces coupled integral equations to algebraic equations and thereby provides a useful intuitive tool. We used this frame-

work to argue that data obtained in lattice simulations of quenched-QCD indicate the existence of net attraction in the color-octet projection of the quark-antiquark scattering kernel.

We observed that the presence of such attraction can materially affect the uniformity of pointwise convergence to solutions of the gap and vertex equations. Our results illustrate that the solutions of two gap equations that are defined via vertex truncations or *Ansätze* which appear similar at spacelike momenta need not yield qualitatively equivalent results for the dressed-quark propagator.

The dependence of our calculated dressed-quark-gluon vertex on the current-quark mass is weak until that mass becomes commensurate in magnitude with the theory's intrinsic mass-scale. For masses of this magnitude and above, vertex dressing is suppressed and the dressed vertex is well approximated by the bare vertex.

The feature that the diagrammatic content of our model for the vertex is explicitly enumerable enabled the systematic construction of quark-antiquark kernels that ensure the preservation of all Ward-Takahashi identities associated with strong interaction observables. This guarantees that the pion is automatically realized as a Goldstone mode in the chiral limit. Such a result is impossible if one merely guesses a form for the vertex.

We illustrated that with increasing current-quark mass the rainbow-ladder truncation provides an increasingly reliable estimate of the model's exact vector meson mass. For pseudoscalar mesons, this is even more true because the rainbow-ladder and exact results are guaranteed by the Ward-Takahashi identity to agree in the chiral limit. Moreover, both in rainbow-ladder truncation and with the complete vertex and kernel, the splitting between pseudoscalar and vector meson masses vanishes as the current-quark mass increases. In our complete model calculation this splitting is 130 MeV at the *c*-quark mass and only 40 MeV at the *b*-quark mass, a pattern which suggests that the pseudoscalar partner of the $\Upsilon(1S)$ cannot have a mass as low as that ascribed currently to the $\eta_b(1S)$.

Color-antitriplet diquark correlations form bound states in rainbow-ladder truncation. However, we demonstrated that introducing a very small amount of repulsion into the kernel eliminates these states from the spectrum. If, on the other hand, one introduces a small amount of color-octet attraction, these diquarks persist as bound states. However, with the amount of attraction suggested by lattice data, diquarks vanish from the spectrum.

ACKNOWLEDGMENTS

We are pleased to acknowledge valuable interactions with R. Alkofer, A. Kızılersü, and F. J. Llanes Estrada. This work was supported by: the Austrian Research Foundation *FWF, Erwin-Schrödinger-Stipendium* No. J2233-N08; the Department of Energy, Office of Nuclear Physics, Contract No. W-31-109-ENG-38; the *A.v. Humboldt-Stiftung* via a *F.W. Bessel Forschungspreis*; and the National Science Foundation under Contract Nos. INT-0129236 and PHY-0301190.

[1] J. Papavassiliou and J. M. Cornwall, Phys. Rev. D **44**, 1285 (1991).
[2] F. T. Hawes, C. D. Roberts, and A. G. Williams, Phys. Rev. D **49**, 4683 (1994).
[3] F. T. Hawes, P. Maris, and C. D. Roberts, Phys. Lett. B **440**, 353 (1998).
[4] M. B. Hecht, M. Oettel, C. D. Roberts, S. M. Schmidt, P. C. Tandy, and A. W. Thomas, Phys. Rev. C **65**, 055204 (2002).
[5] D. Morel and S. Capstick, nucl-th/0204014.
[6] E. J. Hackett-Jones, D. B. Leinweber, and A. W. Thomas, Phys. Lett. B **489**, 143 (2000); **494**, 89 (2000).
[7] C. D. Roberts and A. G. Williams, Prog. Part. Nucl. Phys. **33**, 477 (1994).
[8] P. Maris, C. D. Roberts, and P. C. Tandy, Phys. Lett. B **420**, 267 (1998).
[9] P. Maris and C. D. Roberts, Phys. Rev. C **56**, 3369 (1997).
[10] K. Langfeld, H. Markum, R. Pullirsch, C. D. Roberts, and S. M. Schmidt, Phys. Rev. C **67**, 065206 (2003).
[11] C. D. Roberts and S. M. Schmidt, Prog. Part. Nucl. Phys. **45**, S1 (2000).
[12] R. Alkofer and L. v. Smekal, Phys. Rep. **353**, 281 (2001).
[13] P. Maris and C. D. Roberts, Int. J. Mod. Phys. E **12**, 297 (2003).
[14] D. C. Curtis and M. R. Pennington, Phys. Rev. D **42**, 4165 (1990).
[15] A. Bashir and M. R. Pennington, Phys. Rev. D **53**, 4694 (1996).
[16] J. C. R. Bloch, Few-Body Syst. **33**, 111 (2003).
[17] Z.-h. Dong, H. J. Munczek, and C. D. Roberts, Phys. Lett. B **333**, 536 (1994).
[18] D. Atkinson and P. W. Johnson, Phys. Rev. D **41**, 1661 (1990).
[19] A. G. Williams, G. Krein, and C. D. Roberts, Ann. Phys. (N.Y.) **210**, 464 (1991).
[20] F. T. Hawes and A. G. Williams, Phys. Lett. B **268**, 271 (1991).
[21] H. J. Munczek, Phys. Lett. B **175**, 215 (1986).
[22] C. J. Burden, C. D. Roberts, and A. G. Williams, Phys. Lett. B **285**, 347 (1992).
[23] L. von Smekal, R. Alkofer, and A. Hauck, Phys. Rev. Lett. **79**, 3591 (1997); L. von Smekal, A. Hauck and R. Alkofer, Ann. Phys. (N.Y.) **267**, 1 (1998); **269**, 182 (1998).
[24] D. Atkinson and J. C. R. Bloch, Phys. Rev. D **58**, 094036 (1998); D. Atkinson and J. C. R. Bloch, Mod. Phys. Lett. A **13**, 1055 (1998).
[25] K. I. Kondo, hep-th/0303251.
[26] UKQCD Collaboration, D. B. Leinweber, J. I. Skullerud, A. G. Williams, and C. Parrinello Phys. Rev. D **60**, 094507 (1999); **61**, 079901 (2000).
[27] P. O. Bowman, U. M. Heller, D. B. Leinweber, and A. G. Williams, Nucl. Phys. B (Proc. Suppl.) **119**, 323 (2003).
[28] M. S. Bhagwat, M. A. Pichowsky, C. D. Roberts, and P. C. Tandy, Phys. Rev. C **68**, 015203 (2003).

[29] A. Bender, C. D. Roberts, and L. von Smekal, Phys. Lett. B **380**, 7 (1996).
[30] A. Bender, W. Detmold, A. W. Thomas, and C. D. Roberts, Phys. Rev. C **65**, 065203 (2002).
[31] H. J. Munczek and A. M. Nemirovsky, Phys. Rev. D **28**, 181 (1983).
[32] M. A. Ivanov, Y. L. Kalinovsky, and C. D. Roberts, Phys. Rev. D **60**, 034018 (1999).
[33] P. Bicudo, S. Cotanch, F. Llanes-Estrada, P. Maris, E. Ribeiro, and A. Szczepaniak, Phys. Rev. D **65**, 076008 (2002); P. Bicudo, Phys. Rev. C **67**, 035201 (2003).
[34] S. R. Cotanch and P. Maris, Phys. Rev. D **66**, 116010 (2002); **68**, 036006 (2003).
[35] A. Krassnigg and C. D. Roberts, nucl-th/0308039; A. Höll, A. Krassnigg and C. D. Roberts, nucl-th/0311033.
[36] W. J. Marciano and H. Pagels, Phys. Rep., Phys. Lett. **36**, 137 (1978).
[37] C. D. Roberts, Nucl. Phys. A **605**, 475 (1996).
[38] P. Maris and P. C. Tandy, Phys. Rev. C **61**, 045202 (2000); **62**, 055204 (2000); **65**, 045211 (2002).
[39] A. I. Davydychev, P. Osland, and L. Saks, Phys. Rev. D **63**, 014022 (2001).
[40] J. I. Skullerud, P. O. Bowman, A. Kızılersü, D. B. Leinweber, and A. G. Williams, JHEP **0304**, 047 (2003).
[41] J. S. Ball and T. W. Chiu, Phys. Rev. D **22**, 2542 (1980).
[42] H. J. Munczek, Phys. Rev. D **52**, 4736 (1995).
[43] P. Maris and P. C. Tandy, Phys. Rev. C **60**, 055214 (1999);
[44] D. Kekez and D. Klabučar, Phys. Rev. D **65**, 057901 (2002).
[45] A. Scarpettini, D. Gomez Dumm, and N. N. Scoccola, Phys. Rev. D **69**, 114018 (2002).
[46] Particle Data Group, K. Hagiwara *et al.*, Phys. Rev. D **66**, 010001 (2002); and 2003 off-year partial update for the 2004 edition available at http://pdg.lbl.gov/
[47] P. Maris, in *Quark Confinement and the Hadron Spectrum IV*, edited by W. Lucha and K. Maung Maung (World Scientific, Singapore, 2002).
[48] P. C. Tandy, Prog. Part. Nucl. Phys. **50**, 305 (2003).
[49] C. D. Roberts, Nucl. Phys. B, Proc. Suppl. **108**, 227 (2002).
[50] UKQCD Collaboration, K. C. Bowler *et al.* , Phys. Rev. D **62**, 054506 (2000).
[51] F. J. Llanes-Estrada, S. R. Cotanch, A. P. Szczepaniak and E. S. Swanson, hep-ph/0402253.
[52] M. Ida and R. Kobayashi, Prog. Theor. Phys. **36**, 846 (1966); D. B. Lichtenberg and L. J. Tassie, Phys. Rev. **155**, 1601 (1967).
[53] R. T. Cahill, C. D. Roberts, and J. Praschifka, Aust. J. Phys. **42**, 129 (1989).
[54] M. Oettel, G. Hellstern, R. Alkofer, and H. Reinhardt, Phys. Rev. C **58**, 2459 (1998).
[55] H. Mineo, W. Bentz, and K. Yazaki, Phys. Rev. C **60**, 065201 (1999).
[56] R. T. Cahill, C. D. Roberts, and J. Praschifka, Phys. Rev. D **36**, 2804 (1987).
[57] P. Maris, Few-Body Syst. **32**, 41 (2002).